Biosensors and Bioelectronics 102 (2018) 70–79

Contents lists available at ScienceDirect

Biosensors and Bioelectronics

journal homepage: www.elsevier.com/locate/bios

Label-free electrochemical DNA biosensor for guanine and adenine by ds-DNA/poly(L-cysteine)/Fe_3O_4 nanoparticles-graphene oxide nanocomposite modified electrode

Majid Arvand*, Mona Sanayeei, Shiva Hemmati

Electroanalytical Chemistry Laboratory, Faculty of Chemistry, University of Guilan, Namjoo Street, P.O. Box: 1914-41335, Rasht, Iran

ARTICLE INFO

Keywords:
DNA biosensor
Guanine
Adenine
Nanomaterials
Electroanalytical technique

ABSTRACT

In this study, we aim to design a simple and effective electrochemical DNA biosensor based on a carbon paste electrode modified with ds-DNA/poly(L-cysteine)/Fe_3O_4 nanoparticles-graphene oxide (ds-DNA/p(L-Cys)/Fe_3O_4 NPs-GO/CPE) for sensitive detection of adenine (A) and guanine (G). The electrocatalytic oxidation of A and G on the electrode was explored by differential pulse voltammetry (DPV) and cyclic voltammetry (CV). This sensor shows separated and well-defined peaks for A and G, by which one can determine these biological bases individually or simultaneously. The ds-DNA/p(L-Cys)/Fe_3O_4 NPs-GO/CPE exhibited an increase in peak currents and the electron transfer kinetics and decrease in the overpotential for the oxidation reaction of A and G. Under the optimal conditions a linear relationship is figured out between the peak current and the analytes' concentrations on a range of 0.01–30.0 μM and 0.01–25.0 μM for simultaneous determination of A and G, with detection limits of 3.48 and 1.59 nM, respectively. As well as, individually determination is resulted two linear concentration ranges of 0.01–30.0 μM for A and 0.01–25.0 μM for G with detection limits of 3.90 and 1.58 nM for A and G, respectively. The proposed biosensor exhibited some advantages in terms of simplicity, rapidity, high sensitivity, good reproducibility and long-term stability. Furthermore, the measurements of thermally denatured single-stranded DNA were carried out and the value of (G + C)/(A + T) of DNA was calculated as about 0.77 for various DNA samples. This study also ascertained that the proposed biosensor can be profitable to evaluate DNA bases damage.

1. Introduction

In recent years, there has been an increase in the use of nucleic acids as a tool in the recognition of many compounds by using deoxyribonucleic acid (DNA) as a surface-modification element in electrochemical biosensors (Rezaei et al., 2016). DNA has gained increasing attention as well as their promise in the field of electrochemistry, which plays a vital role to transfer genetic information from one descendant to another (Zeng et al., 2013). Therefore, sequence-specific detection of DNA has been reported important for medical diagnosis of genetic diseases, mutations, molecular biology and forensic science (Esmaeili et al., 2016). The technology of DNA biosensors has been developed to measure the occurrence of DNA hybridization via the matching of complementary bases; adenine-thymine (T) and guanine-cytosine (C) (Tabrizi and Shamsipur, 2015). The electrochemical DNA biosensor is one of the most attractive methods because of their low cost, high sensitivity, rapid response rate, and good selectivity as well as their capacity for instrument miniaturization (Huang et al., 2014). To date, various types of DNA electrochemical biosensors, using a broad range of nanomaterials such as metal nanoparticles and carbon nanomaterials have been utilized to increase performance of DNA biosensors (Peng et al., 2015).

Guanine and adenine are two of the four important bases present in DNA structure and play fundamental roles in the life process (Ensafi et al., 2014). They have effects on coronary and cerebral circulation, control of blood flow, prevention of cardiac arrhythmias, inhibition of neurotransmitter release and modulation of adenylate cyclase activity (Huang et al., 2013). The abnormal changes of the bases in organisms suggest the deficiency and mutation of the immunity system and may indicate the presence of various diseases such as cancer, AIDS, myocardial cellular energy status, disease progress and therapy responses (Chen et al., 2007; Huang et al., 2011). A mutation is a permanent change in the DNA. A mutation can arise spontaneously without apparent cause, or in response to radiation, ultraviolet light, certain chemicals, or viruses. Some mutations involve the substitution of one base pair for another and one or more base pairs can be added to, or

* Corresponding author.
E-mail address: arvand@guilan.ac.ir (M. Arvand).

http://dx.doi.org/10.1016/j.bios.2017.11.002
Received 8 September 2017; Received in revised form 30 October 2017; Accepted 1 November 2017

removed from, the chain. Mutations can lead to cell death, to alterations in the way a cell functions, or in some cases to cancer (Anu Prathap et al., 2013). Therefore, the determination of G and A has great significance to the bioscience and clinical diagnosis. A survey of the literature revealed that many analytical methods have been described for determination of A and G such as high-performance liquid chromatography (Zhou et al., 2015), capillary electrophoresis (Yu et al., 2014), spectroscopic methods (Yari and Saidikhah, 2016), chemiluminescence (Feng et al., 2011) and mass spectrometry (Huang and Chang, 2007). Although these methods are sensitive, but these embrace several shortcomings such as complicated instruments, time-consuming sample pretreatment and also the availability of these high cost instruments in the laboratories are limited (Mirmomtaz et al., 2009). Compared to these methods, electrochemical technique makes a good candidate for the analysis of A and G owing to their practicality, simplicity, rapidity and ease of miniaturization (Palecek and Bartosik, 2012). As well as, the electrochemical methods suffer problems for the detection of nucleic bases such as slow electron transfer kinetics, high overpotential and overlapping of their oxidation peaks (Arvand et al., 2015). To overcome these problems, utilization of chemical modified electrodes is always beneficial. In modifying the biosensor, nanomaterials (NMs) are generally used, due to their enhanced catalytic properties and high electrical conductivity (Kurbanoglu et al., 2017). More active sites and abundant functional groups on the NMs surface lead to high activity for adsorption and catalysis.

Graphene oxide (GO) is one of the most important derivatives of graphene having large surface area, excellent conductivity and strong mechanical strength. These properties make GO a great candidate for electrode modification (Arvand and Gholizadeh, 2013a, 2013b).

Furthermore, magnetic nanoparticles are one kind of new nanostructured materials and have attracted an intensive notice for application in sensors (Arvand and Hemmati, 2017) because of easy synthesis and functionalization, excellent interaction features between reactants and active sites, high surface area, electro-conductivity and biocompatibility (Gu et al., 2014). As an important magnetic material, magnetite (Fe_3O_4) is a common ferrite for the separation of some metal ions (Mashhadizadeh and Karami, 2011) and electrodes modification (Chawla and Pundir, 2011). Recently, the use of polymer modified electrodes has drawn a great attention on the analytical purposes (Ma et al., 2013), due to their selectivity, sensitivity, multiple active sites, strong adherence to the electrode surface and the chemical stability (Ferraz et al., 2016).

L-Cysteine (L-Cys) is an important amino acid present in natural proteins and plays key role in biological systems (Sundaram and Abdul Kadir, 2017). As an electrochemical sensor material, poly cysteine provides abundant active sites for binding analytes, rapid electron transfer and tunable conductivity (Fu et al., 2011).

The broader goal of this work was to develop a new electrochemical protocol with high sensitivity toward A and G which is named ds-DNA/p(L-Cys)/Fe_3O_4 NPs-GO/CPE. Moreover, the study also included a comparative evaluation of modified and unmodified electrodes to assess the contribution of ds-DNA, p(L-Cys), Fe_3O_4 NPs and GO at improving electrochemical detection. Furthermore, real samples of denatured DNA have been proven to produce a good response towards A and G.

2. Materials and methods

2.1. Chemicals and reagents

All reagents and solvents were of the highest purity available from Merck (Darmstadt, Germany) and were used without further purification. Details on the reagents were provided in Supplementary materials.

2.2. Apparatus

Electrochemical measurements were carried out using a PalmSens electrochemical analyzer connected to a personal computer and controlled by PS-Trace 4.5 software. A regular three-electrode system including a modified electrode as working electrode, a saturated Ag/AgCl electrode as reference electrode and a platinum wire as counter electrode was used to obtain the electrochemical data. The pH of the solutions was adjusted by a model 827 pH meter (Metrohm, Swiss).

Atomic force microscopy (AFM; NTEGRA, NT-MDT, TS-150), Field emission scanning electron microscope (FE-SEM; Sigma, Zeiss, Germany), Fourier transform infrared spectrometer (FT-IR; Shimadzu 8900, Kyoto, Japan), X-ray diffraction spectrometer (XRD, Philips PW1840), transmission electron microscope (TEM; Philips) and scanning electron microscope (SEM, Electroanalyzer Sama 500) were used to characterize the morphology, size and structure of the nanomaterials and nanocomposite.

2.3. Synthesis of GO

GO was synthesized from pure graphite powder via the modified Brodie method (Arvand and Gholizadeh, 2013a, 2013b). The experimental procedures were described in Supplementary data.

2.4. Synthesis of Fe_3O_4 NPs

Fe_3O_4 NPs were prepared according to the modified Massart method (Mohammad-Rezaei et al., 2014) via the co-precipitation of a mixture of $FeCl_3{\cdot}6H_2O$ and $FeCl_2{\cdot}4H_2O$ under N_2 atmosphere. The complete experimental procedures were described in Supplementary data.

2.5. Preparation of modified electrodes

For preparation of a carbon paste electrode, graphite powder, paraffin, a Teflon tube (*ca.* 3 mm i.d. and 10 cm long) and a copper wire were used. Carbon paste was prepared by mixing of graphite powder and paraffin using a mortar and pestle. The carbon paste modified with Fe_3O_4 NPs-GO was prepared by mixing optimized amounts of graphite powder, GO and Fe_3O_4 NPs with appropriate amount of paraffin oil. Then the paste was packed into a Teflon tube and a copper rod was embedded into the paste to provide electrical connection. Before measurement, the electrode surface was smoothened on a piece of transparent paper to get a smooth and fresh surface.

The electro-polymerization of L-Cys on the Fe_3O_4 NPs-GO/CPE surface was carried out by CV technique with using a 0.1 M PBS (pH = 7.0) containing 7.5 mM L-Cys throughout 8 cycles in the potential range from –1.5 to + 2.0 V at a scan rate of 100 mV s^{-1}.

The ds-DNA/p(L-Cys)/Fe_3O_4 NPs-GO/CPE was prepared by drop casting of 6.0 μL ds-DNA solution on surface electrode and subsequently air drying at room temperature. The overall fabrication process of the ds-DNA/p(L-Cys)/Fe_3O_4 NPs -GO/CPE is presented in Scheme 1.

2.6. Real samples preparation

DNA samples were simply denaturized by thermally treatment according to the literature (Wang et al., 2006). The hydrogen bonds of ds-DNA will be ruptured during this thermal process. In short, 3.0 mg DNA of human blood, hen blood and Anoxybacillus bacteria was digested using 1.0 mL of 1.0 M HCl in a sealed glass tube. After heating in boiling water bath (100 °C) for 80 min, 1.0 mL of 1.0 M NaOH was added. Finally, the solution was rapidly cooled in an ice bath. Then, known volume of the resulted solutions was diluted using 0.1 M ABS (pH = 5.6). Bladder cancer patient' blood DNA sample was also prepared by above method as a damaged DNA sample.

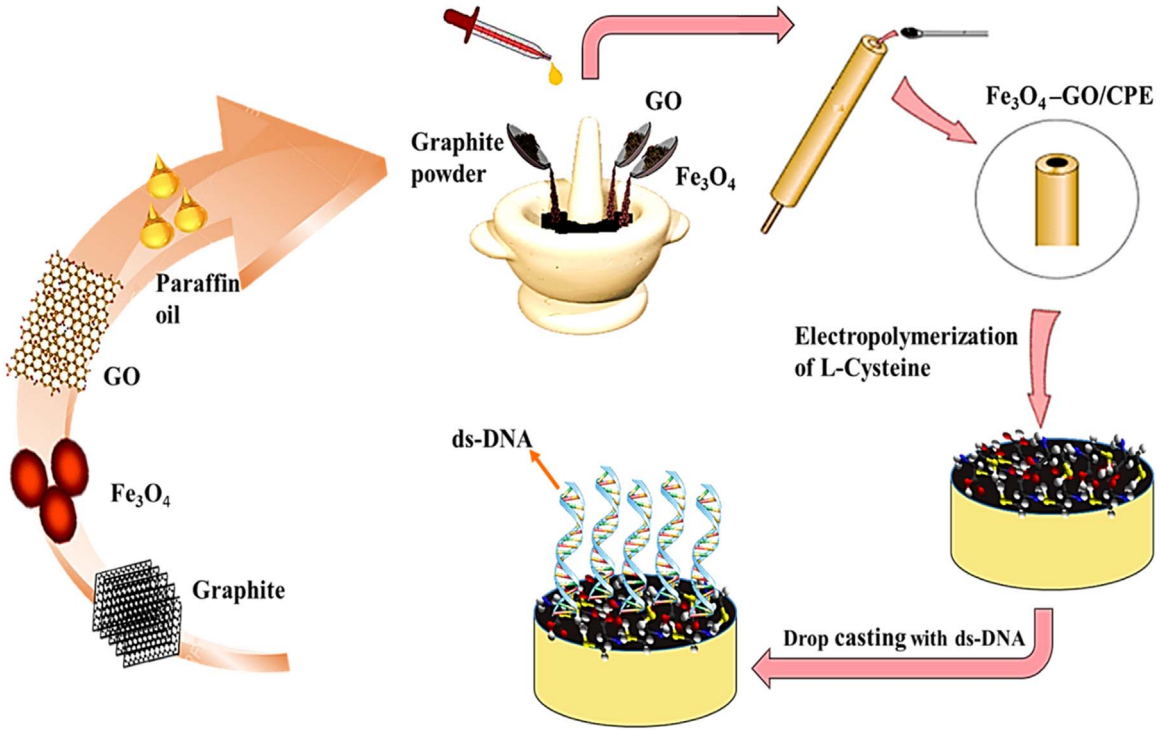

Scheme 1. Schematic representation for the fabrication process of the ds-DNA/p(L-Cys)/Fe_3O_4 NPs-GO/CPE.

3. Results and discussion

3.1. Characterization

Fig. 1A indicates the XRD pattern of Fe_3O_4 NPs. In Fig. 1A, the diffraction peaks at 30.26°, 35.67°, 43.21°, 53.63°, 57.34° and 62.88° are in agreement with standard XRD card of Fe_3O_4 (Mohammad-Rezaei et al., 2014).

The TEM image of Fe_3O_4 NPs (Fig. 1B) shows the particles are agglomerated by irregular shaped and the size of the particles is in the nanometer range.

The morphology of GO-Fe_3O_4 composite material is shown by the TEM image in Fig. S1. The image signifies that the surface of GO are densely sheltered with uniformly distributed black colored Fe_3O_4 nanoparticles. The Fe_3O_4 nanoparticles are distributed on GO sheet in such a manner there is not much agglomeration of Fe_3O_4 nanoparticles.

The FT-IR spectrum of GO (Fig. 1C) shows the broad and intense peaks about 3500 cm^{-1} which is characteristic of O–H groups. The peaks at 1718, 1622, 1361, 1242, and 1078 cm^{-1} are attributed to the C=O, C=C, C–O, C–OH and C–O stretching, respectively. The above FT-IR data confirms that there are oxygen-containing functional groups on GO surface which resulted from the oxidization, hydroxylation and carboxylation of the graphite (Arvand and Gholizadeh, 2013a, 2013b). Fig. 1D shows SEM image of GO. It is apparent that GO nanosheets are flake-like with exposed sharp edges. These observations indicate that GO nanosheets were successfully synthesized and porous network of GO sheets increase the effective surface area.

The morphologies of p(L-Cys) and ds-DNA/p(L-Cys)/Fe_3O_4 NPs-GO were characterized by FE-SEM. As illustrated in Fig. 1E, by electropolymerization of L-Cys polymer layer with multiple bumps and protuberances was conformed. The surface of ds-DNA/p(L-Cys)/Fe_3O_4 NPs-GO composite film (Fig. 1F) was quite monotonic and presented a curly morphology consisting of a dendritic structure. Thus, it can be resulted that ds-DNA chains deposited successfully.

AFM was used to study the surface topography of the p(L-Cys) (Fig. 1G) and ds-DNA/p(L-Cys)/Fe_3O_4 NPs-GO (Fig. 1H) modified electrodes. The AFM image of p(L-Cys) reveals that this polymeric film is composed of many granular particles which led to a significant increase in the effective surface area for loading the ds-DNA. In Fig. 1G and H, the obvious morphological change between p(L-Cys) and ds-DNA/p(L-Cys)/Fe_3O_4 NPs-GO modified electrodes can be observed which results in decrement of both bumps and the surface roughness by immobilizing ds-DNA on the p(L-Cys) film. In other words the AFM results show that the ds-DNA/p(L-Cys)/Fe_3O_4 NPs-GO has a more compact and denser structure than the pristine p(L-Cys). Further analysis indicated that the p(L-Cys) surface has an average roughness of 93.5 nm, whereas ds-DNA/p(L-Cys)/Fe_3O_4 NPs-GO surface accounts for an average roughness of 68.2 nm. As reported in literatures the compact structure of a conductive polymer allows the conductive areas in the polymer to become more connected (Cho et al., 2014).

3.2. Electrochemical properties of ds-DNA/p(L-Cys)/Fe_3O_4 NPs-GO/CPE

The electrochemical performances of CPE, GO/CPE, Fe_3O_4 NPs-GO/CPE, p(L-Cys)/Fe_3O_4 NPs-GO/CPE andds-DNA/p(L-Cys)/Fe_3O_4 NPs-GO/CPE were investigated under the identical conditions using a solution of 5.0 mM $K_3[Fe(CN)_6]/K_4[Fe(CN)_6]$ containing 0.1 M KCl. As shown in Fig. 2A, a pair of redox peaks were observed at CPE (curve *a*), GO/CPE (curve *b*), Fe_3O_4 NPs-GO/CPE (curve *c*), p(L-Cys)/Fe_3O_4 NPs-GO/CPE (curve *d*) and ds-DNA/p(L-Cys)/Fe_3O_4 NPs-GO/CPE (curve *e*), respectively. It can also be observed that the magnitude of redox peak current for $K_3[Fe(CN)_6]/K_4[Fe(CN)_6]$ couple has been enhanced at modified electrodes compared to bare electrode. This phenomenon could be attributed to the increased accessible active sites and faster electron transfer kinetics caused by the co-contribution of GO-Fe_3O_4 NPs and conducting polymer. Besides, the redox peak currents at ds-DNA/p(L-Cys)/Fe_3O_4 NPs-GO/CPE in comparison with p(L-Cys)/Fe_3O_4 NPs-GO/CPE significantly decreased, which could be explained in terms of the electrostatic repulsion of the negative charges in phosphate groups existing in DNA structure towards the negative charges existing in $[Fe(CN)_6]^{3-}/[Fe(CN)_6]^{4-}$ ions.

Electrochemical impedance spectroscopy (EIS) was used to monitor the change of the electrode surface during the modification process. The EIS includes a semicircular part and a linear part. The semicircular part

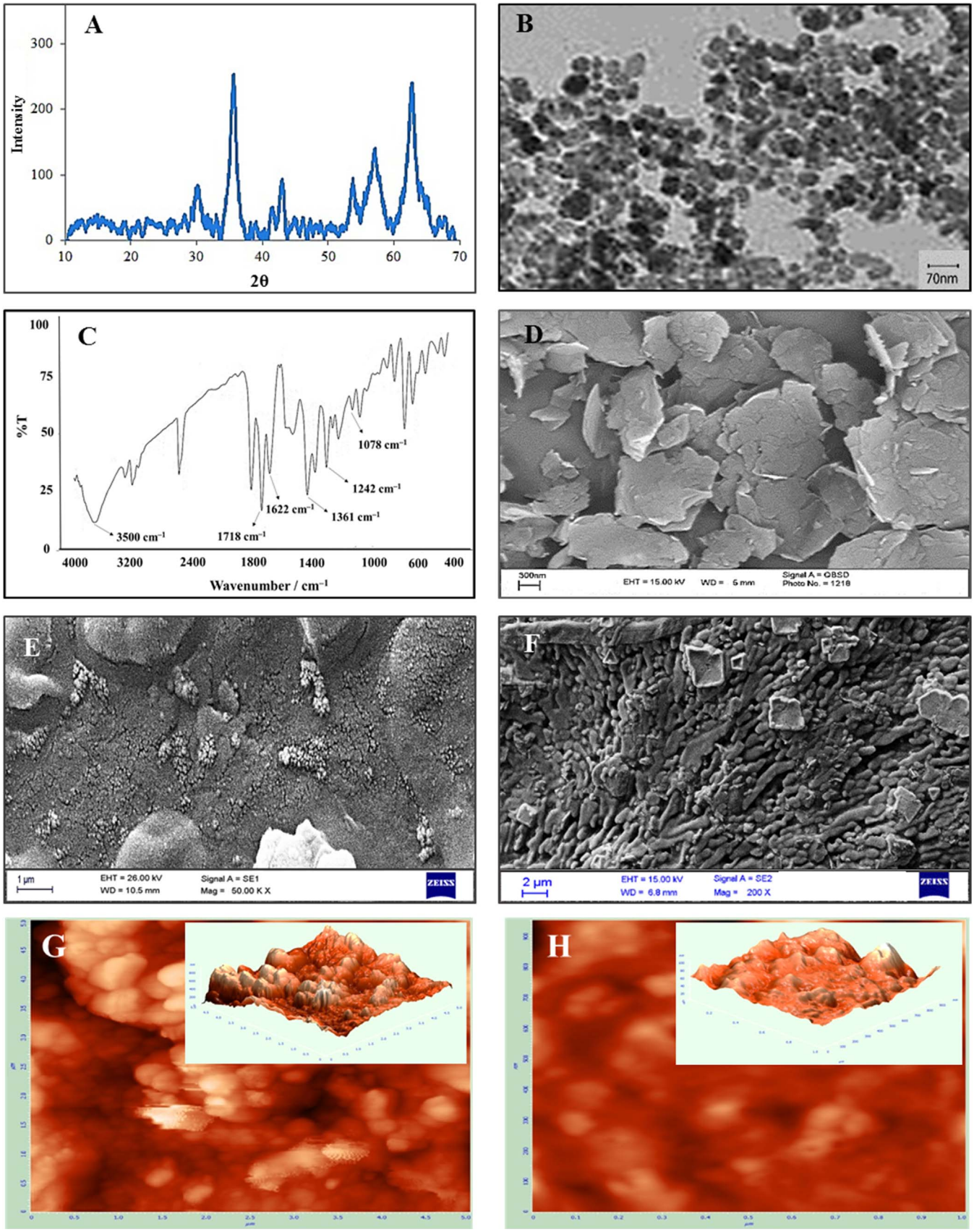

Fig. 1. (A) XRD pattern of Fe_3O_4 NPs; (B) TEM image of Fe_3O_4 NPs; (C) FT-IR spectrum of GO nanosheets; (D) SEM image of GO nanosheets. FE-SEM images of (E) p(L-Cys) and (F) ds-DNA/p(L-Cys)/Fe_3O_4 NPs-GO. Two-dimensional AFM topography images of (G) p(L-Cys) and (H) ds-DNA/p(L-Cys)/Fe_3O_4 NPs-GO. Insets show the three-dimensional AFM topography images of p(L-Cys) and ds-DNA/p(L-Cys)/Fe_3O_4 NPs-GO.

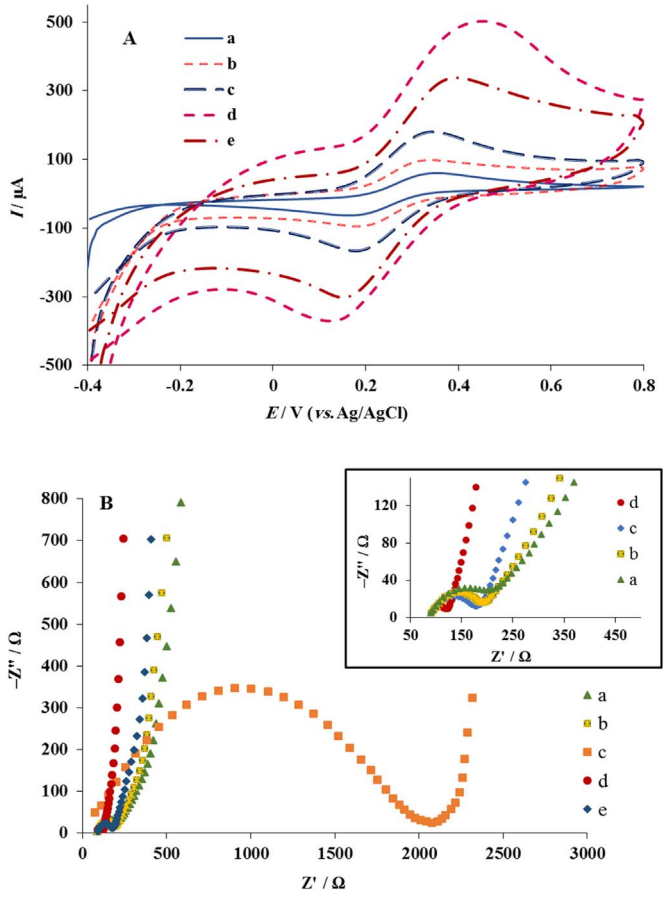

Fig. 2. (A) CVs of 5.0 mM $K_3[Fe(CN)_6]/K_4[Fe(CN)_6]$ in 0.1 M KCl obtained at scan rate of 100 mV s^{-1}. Curve *a*: bare CPE, curve *b*: GO/CPE, curve *c*: Fe_3O_4 NPs-GO/CPE, curve *d*: p(L-Cys)/Fe_3O_4 NPs-GO/CPE, curve *e*: ds-DNA/p(L-Cys)/Fe_3O_4 NPs-GO/CPE. (B) Nyquist diagrams in a solution containing 5.0 mM $K_3[Fe(CN)_6]/K_4[Fe(CN)_6]$ and 0.1 M KCl at (*a*) CPE, (*b*) GO/CPE, (*c*) Fe_3O_4 NPs-GO/CPE, (*d*) p(L-Cys)/Fe_3O_4 NPs-GO/CPE, (*e*) ds-DNA/p(L-Cys)/Fe_3O_4 NPs-GO/CPE.

at higher frequencies corresponds to the electron transfer limited process, and the diameter is equivalent to the electron transfer resistance (R_{ct}), which reflects the electron transfer kinetics of the redox probe at the electrode interface. The linear part at lower frequencies corresponds to the diffusion process. Fig. 2B demonstrates the Nyquist plots of the EIS obtained in 5.0 mM $K_3[Fe(CN)_6]/K_4[Fe(CN)_6]$ solution at the bare CPE, GO/CPE, Fe_3O_4 NPs-GO/CPE, p(L-Cys)/Fe_3O_4 NPs-GO/CPE and ds-DNA/p(L-Cys)/Fe_3O_4 NPs-GO/CPE. As shown in Fig. 2B, by modification of bare electrode with GO and Fe_3O_4 NPs-GO, the surface of electrode is improved and due to its high surface area and high conductivity of GO and Fe_3O_4 NPs, R_{ct} is decreased compared to the bare CPE (curves *a*, *b* and *c*). By deposition of p(L-Cys) layer on the surface of electrode, R_{ct} is decreased because the electrode surface is covered by p(L-Cys), which improves the electron transfer between probe and the surface of electrode (curve *d*). The amount of R_{ct} is increased by immobilization of ds-DNA on the p(L-Cys)/Fe_3O_4 NPs-GO/CPE surface (curve *e*), due to the electrostatic repulsion force between the negatively charged $[Fe(CN)_6]^{3-}/[Fe(CN)_6]^{4-}$ and ds-DNA and preventing $[Fe(CN)_6]^{3-}/[Fe(CN)_6]^{4-}$ ions from reaching to the electrode surface occurs.

3.3. Electro-oxidation of A and G

In order to investigate the role and electrocatalytic activity of different working electrodes, we decided to investigate the application of an optimized electrode to measure some purine-base compounds. The electro-oxidations of G and A (100 µM) in 0.1 M CBS-PBS buffer solution (pH 6.5) at a scan rate of 100 mV s^{-1} were examined by using CV. The results are shown in Fig. 3. As can be seen, the voltammograms of G and A bases exhibit just two small peaks with weak intensity at bare CPE (curve *a*) which indicates the slow electron transfer kinetics of G and A. Nevertheless, compared with a bare CPE, the oxidation peak currents of G and A increase at the GO/CPE (curve *b*) and Fe_3O_4 NPs-GO/CPE (curve *c*). This phenomenon returns to the catalytic role of Fe_3O_4 NPs on the oxidation of G and A and to the enhancement of surface area by GO nanosheets. Moreover, the oxidation peak currents of G and A increase significantly at p(L-Cys)/Fe_3O_4 NPs-GO/CPE (curve *d*) and the ds-DNA/p(L-Cys)/Fe_3O_4 NPs-GO/CPE (curve *e*). These significant improvements in electrochemical sensitivity could be caused by two major factors: (1) ds-DNA provides more active sites and facilitates electron transfer between the electrode and species (2) p(L-Cys) itself has good catalytic ability and improve mass transport. As illustrated in Fig. 3 (curve *e*) the peak-to-peak separation between G and A is 280 mV, which is large enough for their simultaneous detection in a mixture. As respects to the enhancement of G and A electro-oxidation

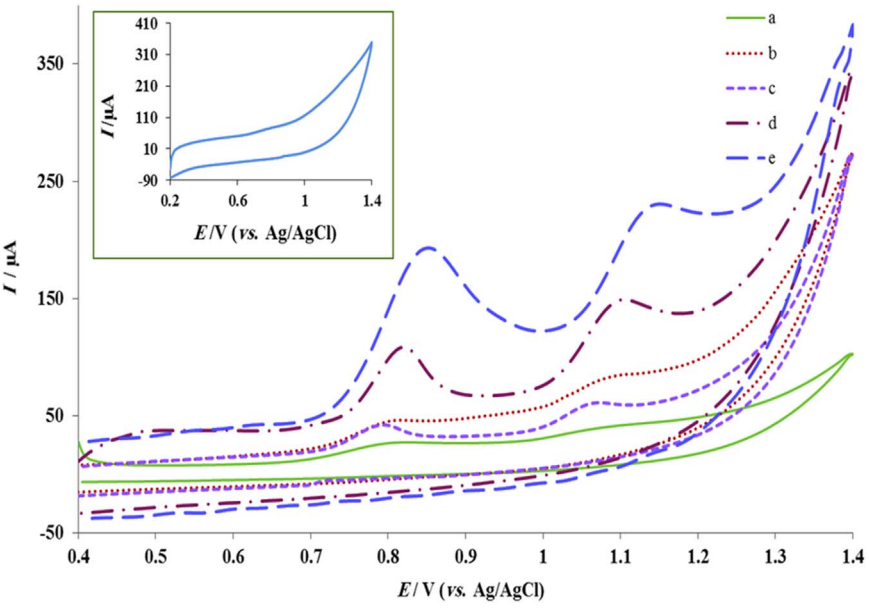

Fig. 3. CVs of 100 µM A and G in CBS-PBS of pH 6.5 obtained at (*a*) bare CPE, (*b*) GO/CPE, (*c*) Fe_3O_4 NPs-GO/CPE, (*d*) p(L-Cys)/Fe_3O_4 NPs-GO/CPE and (*e*) ds-DNA/p(L-Cys)/Fe_3O_4 NPs-GO/CPE. Inset: CV of ds-DNA/p(L-Cys)/Fe_3O_4 NPs-GO/CPE in CBS-PBS of pH 6.5.

signals relative to the unmodified electrode and peak-to-peak separation, it could be concluded that ds-DNA/p(L-Cys)/Fe_3O_4 NPs-GO nanocomposite represents good electrocatalytic behavior for oxidation of analytes, together with the synergistic effect of the adsorption ability of ds-DNA through the base-pairing role and the electrocatalytic property of p(L-Cys) toward G and A (Feng et al., 2011). Moreover, a DNA molecule is considered to be an array of stacked π electrons, which can provide a rapid pathway for electronic charge transport to target molecules due to intercalative and electrostatic binding. The DNA layer could interact with G and A molecules through π–π interactions and also the DNA layer could attract cationic A and G to the interface compounds. Moreover, chemical functionalities of DNA layer could provide a selective interface via hydrogen bonds with the proton-donating group of the G and A (Zou et al., 2012; Rezaei et al., 2016).

3.4. Optimization of modified electrode preparation

3.4.1. Optimization of carbon paste electrode composition

In order to find the best composition of modified electrode, the amount of different components of CPE, including Fe_3O_4 NPs and GO nanosheets were changed in the fixed conditions of voltammetric determination (Fig. 4A). The optimum amount of both Fe_3O_4 NPs and GO was chosen 27 wt% in the paste. Detailed information can be found in Supplementary information.

3.4.2. Effect of L-Cys concentration

The concentration of L-Cys monomer used for the modification of Fe_3O_4 NPs-GO/CPE was studied in the range of 1.0–10 mM. The results are shown in Fig. 4B. The optimum concentration of L-Cys monomer was selected to be 7.5 mM. Detailed information can be observed in Supplementary information.

3.4.3. Effect of number of cycles and scan rates of electro-polymerization

The effect of the thickness of the p(L-Cys) film on the anodic peak currents of A and G were evaluated. The film thickness can be easily controlled by the number of cycles and the scan rate of electro-synthesis. The current responses of both bases reached maximum value at 8 cycles (Fig. 4C). Also effect of scan rates of electro-polymerization was investigated by CV for 8 cycles using potential cycling at different scan rates. Therefore, the scan rate of 0.1 V s^{-1} was optimum for p(L-Cys) layer preparation in the following investigation (Fig. 4D). Detailed information can be found in Supplementary information.

3.4.4. Effect of ds-DNA concentration on immobilization at p(L-Cys)/Fe_3O_4 NPs-GO/CPE surface

The electrochemical DNA biosensor was prepared by immobilizing ds-DNA on the p(L-Cys)/Fe_3O_4 NPs-GO/CPE surface. The optimum amount of 100 ng μL^{-1} of ds-DNA was selected and used in all the further experiments (Fig. 4E). Detailed information can be found in Supplementary information.

3.5. Effect of supporting electrolyte and pH on the electrochemical behavior of A and G

In order to understand the influence of supporting electrolyte on the cyclic voltammetric behaviors of G and A, four kinds of supporting electrolyte solutions were examined (0.1 M of acetate, phosphate, citrate and citrate-phosphate buffer solutions). The better resolution and well-defined oxidation peaks accompanied by lower background levels and highest anodic peak currents of A and G were observed in CBS-PBS. Hereby, the citrate-phosphate buffer was chosen for the rest of studies.

It is essential to examine the influence of pH on electrochemical systems because the pH of the electrolyte medium is one of the variables that strongly influence the voltammograms. We used CV (Fig. S2A) to verify the electrochemical behavior of 100 μM G and A at various pHs from 4.0 to 7.5 in CBS-PBS. Fig. S2B illustrates that the anodic peak currents of G and A increased by raising pH and they achieved to maximum values at pH 6.5 and then leveled off. Therefore, CBS-PBS pH 6.5 was selected as the electrolyte for subsequent experiments.

In this study, it is observed that the oxidation peak potentials of A and G shift negatively with the increase of solution pH in the range of 4.0–7.5. Fig. S2C indicates the dependence of oxidation peak potentials of G and A to pH and the participation of protons in the electrode reaction. A plot of this function shows that the regression equations for G and A are $E_{pa}(V) = -0.052\ pH + 1.16$ ($R^2 = 0.9922$) and $E_{pa}(V) = -0.068\ pH + 1.54$ ($R^2 = 0.9932$), respectively. The slopes of −0.052 and −0.068 (V pH^{-1}) were near to the expected theoretical Nernstian value of 0.059 V pH^{-1}, which implies that numbers of protons and electrons involved in the electrode reaction process is in the ratio 1:1 according to Nernst equation ($0.059m/n$) (Ma and Chen, 2015).

3.6. Effect of scan rate on the peak currents of G and A

In order to investigate the electrochemical reaction mechanism, the experiment of peak current responses of A and G on ds-DNA/p(L-Cys)/Fe_3O_4 NPs-GO/CPE was carried out with CV in various scan rates ranging from 0.02 to 0.14 V s^{-1} (Fig. S3A). The oxidation peak potentials shifted towards relatively positive potential and peak currents of analytes increased linearly with the increase of υ (Fig. S3B), indicating the irreversible electrode reaction and also demonstrating the oxidation of G and A was controlled by adsorption-controlled process. The linear regression equation for G and A can be expressed as $I_{pa}(\mu A) = 698.7\upsilon$ (V s^{-1}) + 4.35 ($R^2 = 0.9964$) and $I_{pa}(\mu A) = 552.1\upsilon$ (V s^{-1}) + 5.91 ($R^2 = 0.9924$), respectively.

The surface concentration (Γ, mol cm^{-2}) of electroactive A and G on ds-DNA/p(L-Cys)/Fe_3O_4 NPs-GO/CPE and bare CPE, can be estimated from the slope of the plot of I_{pa} versus scan rate (Fig. S3B) by (Wang, 2006):

$$I_p = n^2F^2\nu A\Gamma/4RT \quad (1)$$

where n is the number of electrons transferred, F (C mol^{-1}) is the Faraday's constant, A (cm^2) is the area of the electrode, Γ is the surface concentration of the electroactive substance and ν (V s^{-1}) is the scan rate. Based on the slope of the plot of I_p *vs.* ν, the surface concentrations on the ds-DNA/p(L-Cys)/Fe_3O_4 NPs-GO were estimated to be 3.50×10^{-3} μmol cm^{-2} and 4.40×10^{-3} μmol cm^{-2} for A and G, respectively, which were larger than the corresponding values 1.5×10^{-3} μmol cm^{-2} and 1.4×10^{-3} μmol cm^{-2} on bare CPE. The obtained results can imply that the existence ds-DNA/p(L-Cys)/Fe_3O_4 NPs-GO nanohybrid providing a large active surface area and promoting the electron transfer between the biomolecules and the electrode surface for both electroactive species.

3.7. Effect of accumulation parameters

To obtain the excellent performance of the prepared ds-DNA/p(L-Cys)/Fe_3O_4 NPs-GO/CPE the accumulation buffer, accumulation potential (E_{acc}) and accumulation time (t_{acc}) were optimized. The detailed information can be found in Supplementary data.

3.8. Individual determination of G and A using ds-DNA/p(L-Cys)/Fe_3O_4 NPs-GO/CPE

Analytical performance of ds-DNA/p(L-Cys)/Fe_3O_4 NPs-GO/CPE for individual determination of G and A was evaluated with DPV. Under the optimum conditions, mixtures of two bases were prepared, in which the concentration of one base changed gradually, whereas the concentration of another base was kept constant. Fig. 5A demonstrates the typical DPVs with different concentrations of A and constant concentration of G (3.0 μM). The peak current of A increased linearly with

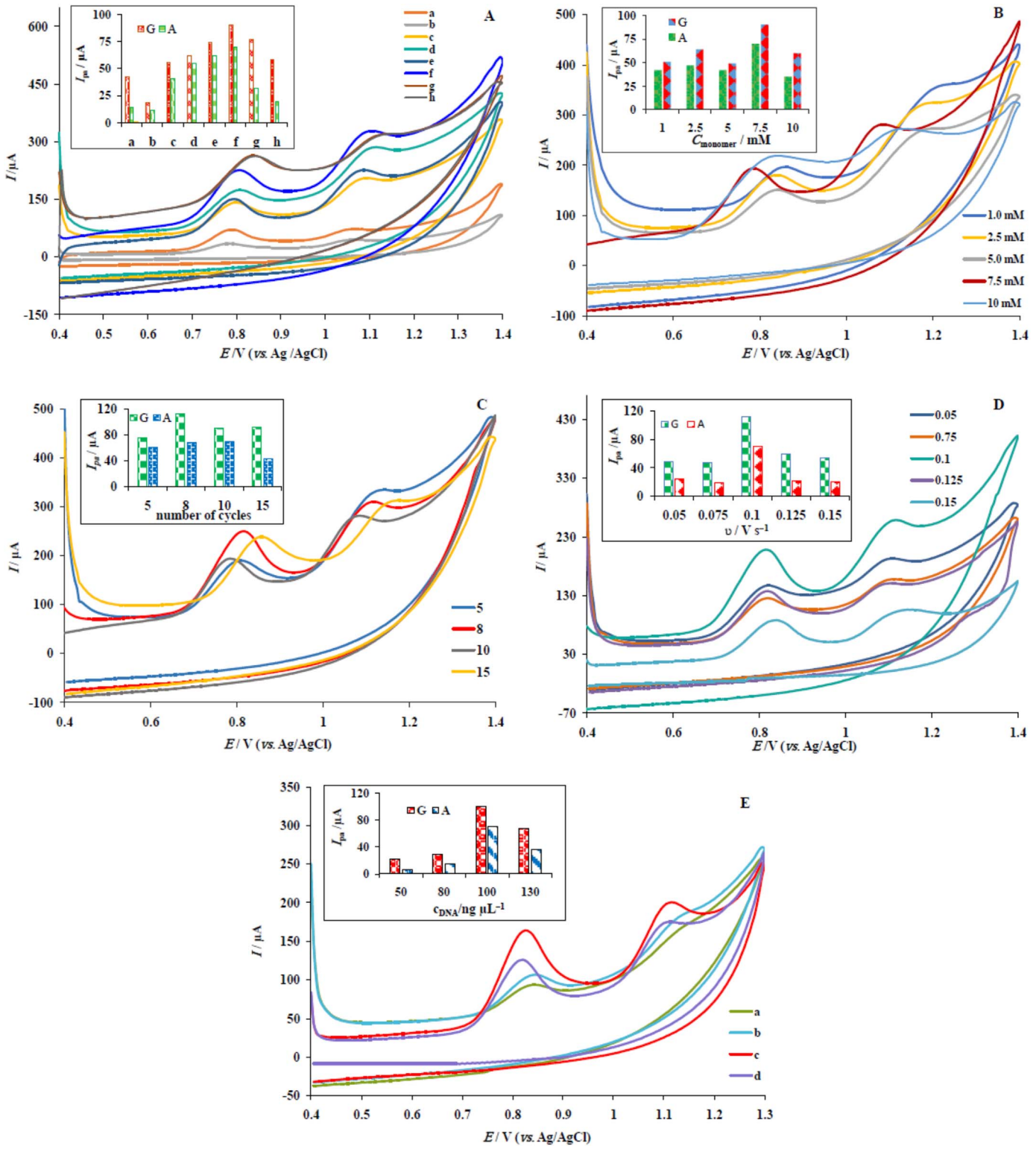

Fig. 4. The influence of (A) amount of Fe_3O_4 NPs-GO employed in the carbon paste (12.5% Fe_3O_4 + 12.5% GO (*a*), 17.5% Fe_3O_4 + 11.76% GO (*b*), 11.76% Fe_3O_4 + 17.5% GO (*c*), 16.66% Fe_3O_4 + 16.66% GO (*d*), 20% Fe_3O_4 + 20% GO (*e*), 27% Fe_3O_4 + 27% GO (*f*), 30% Fe_3O_4 + 30% GO, (*g*) 33.5% Fe_3O_4 + 33.5% GO (*h*), (B) L-Cys monomer concentration, (C) number of cycles of electro-polymerization, (D) scan rate of electro-polymerization, (E) ds-DNA concentration (50 ng μL^{-1} (*a*), 80 ng μL^{-1} (*b*), 110 ng μL^{-1} (*c*), 130 ng μL^{-1} (*d*)) on the peak currents of G and A (100 µM) in 0.1 M CBS-PBS at ds-DNA/p(L-Cys)/Fe_3O_4 NPs-GO/CPE.

an increase in its concentration (inset of Fig. 5A) over the first linear dynamic range of 0.01–5.0 µM and the second was 5.0–30.0 µM with regression equations of I_{pa}(µA) = 1.47*C* (µM) + 1.68 and I_{pa}(µA) = 0.46*C* (µM) + 6.46. The reason for two linear regions may be as follows: At higher concentration than 5 µM, saturation took place and this defined the decrease in the current or a transport mechanism altered. The difference in the slopes for the calibration curves is probably due to the different activity of the electrode surface. In the lower A concentration, due to a high number of active sites the slope of the first calibration curve is high while in the higher A concentration, due to

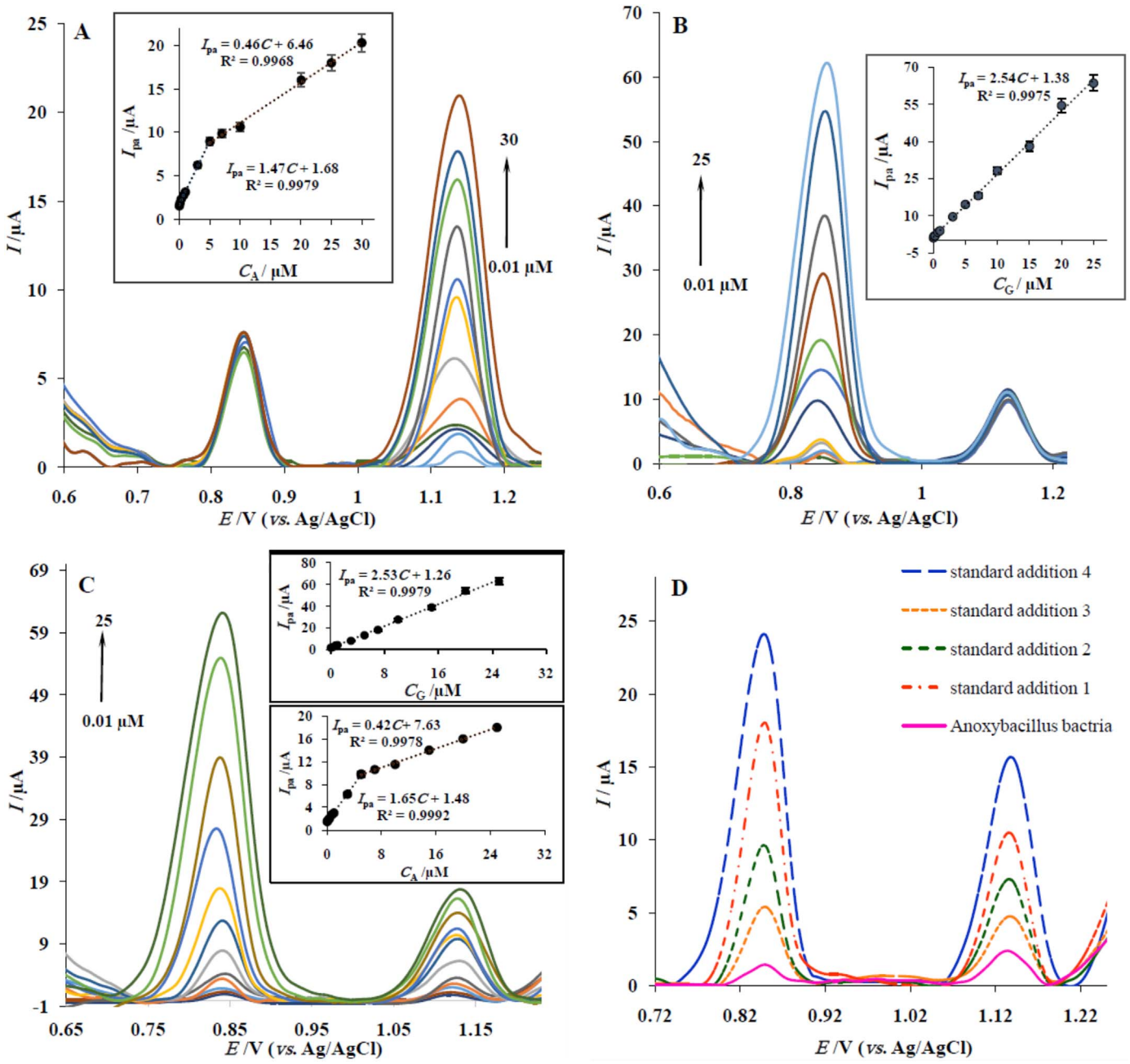

Fig. 5. (A) DPVs of A with concentrations ranging from 0.01 to 30 µM, in the presence G of 3.0 µM in CBS-PBS (pH = 6.5), (B) DPVs of G with concentrations ranging from 0.01 to 25.0 µM, in the presence A of 7.0 µM in CBS-PBS (pH = 6.5). (C) Different concentrations of A and G in the range of 0.01–25.0 µM in CBS-PBS (pH 6.5). Insets show the linear relationship of the peak currents against concentration of the analytes. Error bar: standard deviation for $n = 3$. (D) DPVs obtained for denatured DNA of Anoxybacillus bacteria in CBS-PBS (pH 6.5) before and after spiking with different concentrations of A and G.

decreasing active sites the slope of the second calibration decreased (Mokhtari et al., 2012). Similarly, in different concentrations of G and constant concentration of A (7.0 µM), the peak current of G increased linearly with an increase in its concentration in the linear range of 0.01–25.0 µM and regression equation of I_{pa}(µA) = 2.54C (µM) + 1.38 (inset of Fig. 5B).

The DPV peak of one species was unaltered and the peak current remains constant where the peak current of another species enhanced with increasing concentration. Therefore, it is confirming that ds-DNA/p(L-Cys)/Fe_3O_4 NPs-GO/CPE can be used for the simultaneous determination of A and G, because the oxidation peaks of these two bases are clearly independent from each other. In addition, the limit of detection of the present sensor ($3S_b/m$, S_b is the standard deviation of the blank and m is the slope of the regression line of the calibration curve) for individual determination of A and G were calculated to be 3.9 and 1.58 nM, respectively.

3.9. Simultaneous determination of A and G

Fig. 5C is the DPVs obtained when the concentrations of A and G simultaneously increased. The inset of Fig. 5C shows the linear range of the dependence of the DPV peak currents on the concentration of G and A. The DPV experiments showed that the curves of current versus concentration of either G or A exhibited good linearity in the range of 0.01–25.0 µM. The regression equation for G was I_{pa}(µA) = 2.53C (µM) + 1.26 and the detection limit was achieved 1.59 nM. The regression equation in the linear range of 0.01–5.0 µM for A was I_{pa}(µA) = 1.65C (µM) + 1.48 and in the linear range of 5.0–25.0 µM was I_{pa}(µA) =

0.42*C* (μM) + 7.63 and the detection limit was obtained 3.48 nM. Compared with other modified sensors listed in Table S1, it can be seen that the ds-DNA/p(L-Cys)/Fe_3O_4 NPs-GO/CPE exhibited a wider linear range and lower detection limit in comparison with other reported results.

3.10. Repeatability, reproducibility, response time and stability studies

For validation of the proposed method, various parameters such as repeatability, reproducibility and stability of the analysis were evaluated. The electrode capability for the generation of a repeatable response is defined as the repeatability of the sensor. The repeatability was examined by the detection of 10.0 μM G and A in CBS-PBS (pH 6.5) for six successive determinations. The peak currents were nearly constant with only small relative standard deviations (RSD) of 2.5% and 3.4% for G and A, respectively, indicating good repeatability. Furthermore, under the same procedure, six ds-DNA/p(L-Cys)/Fe_3O_4 NPs-GO/CPE were prepared independently and the fabrication reproducibility was also estimated. The RSD of the peak currents is 3.5% and 4.2% in 10.0 μM G and A in CBS-PBS (pH 6.5), respectively, which demonstrates the reliability of the fabrication procedure.

The response time of the sensor which can be obtained by the *I–t* plots was defined as the time after analyte addition for the sensor's response to reach from 10% to 90% of its final value. The response times of the proposed sensor toward G and A were achieved from the amperograms 2.1 and 1.5 s, respectively.

The lifetime of the developed electrochemical sensor is of particular concern, as the nanocomposite coating may wear off during the stirring and cleaning period. In order to demonstrate the sensing stability of ds-DNA/p(L-Cys)/Fe_3O_4 NPs-GO/CPE, the electro-oxidation responses were assessed by DPV in CBS-PBS buffer solution containing 10.0 μM of G and 20.0 μM of A. The repetitive work was done for 85 times (Fig. S4). The results demonstrate that the peak currents decreased gradually as the number of scans increasing and after 85 continuous cycles, it dropped to 91.0% and 90.9% of the initial values for G and A, respectively, which indicate the great stability of ds-DNA/p(L-Cys)/Fe_3O_4 NPs-GO/CPE for their simultaneous detection, for continuous operation.

The storage stability of ds-DNA/p(L-Cys)/Fe_3O_4 NPs-GO/CPE was verified by measuring the oxidation peak current at A and G concentration of 10.0 μM. By preserving the as-prepared electrode at 4 °C over a period of 3 weeks, the current responses of G and A approximately 91.1% and 94.5% of the original values could still be observed. The eligible decrease in the electrode's response (less than 10%) indicated its satisfactory stability.

3.11. Interference study

The selectivity of the electrochemical sensor was investigated for needed selectivity for determination of the purine bases in the presence of some interfering substances in a solution containing 10.0 μM of G and A. As presented in Table S2, the results specify that up to 1000-fold concentrations of glycine, glucose, uric acid, inorganic ions containing Na^+, K^+, NH_4^+, Ca^{2+}, Mg^{2+}, Cl^-, NO_3^-, SO_4^{2-} and alanine, 500-fold of thymine, 400-fold of leucine, 300-fold of ascorbic acid and methionine, 100-fold of arginine and cytosine and 50-fold of folic acid are tolerable and without significant interferences on the detection of G and A (signal changes were less than 5%). The DPV peak currents of A and G in the absence (I_0) and the presence (I) of interfering agents and relative peak current changes as $[(I/I_0) - 1] \times 100$ are listed in Table S2. We see, except tryptophan, other tested agents have no considerable influence on peak currents of the purine bases. However, the presence of 30-fold molar excess of tryptophan could obviously change the DPV signals of both A and G. In addition, effect of mentioned interfering species on the oxidation signal of 10.0 μM G and A on the ds-DNA/p(L-Cys)/Fe_3O_4 NPs-GO/CPE surface is presented in Fig. S6. The proposed method appears to be selective for simultaneous determination of G and A in real samples.

3.12. Analytical application

3.12.1. Analysis of human blood, hen blood and Anoxybacillus bacteria DNA samples

Inasmuch as, the bases are embedded in the interior of the double helix and existence of the crowded phosphate group on the exterior of the helix, their detection is sterically hindered. The thermally denatured treatment results in an unwinding of duplex DNA and renders the G and A residues more accessible to the electrode surface owing to the increased flexibility in its structure. In this work, in order to evaluate the validity of the proposed method, the ds-DNA/p(L-Cys)/Fe_3O_4 NPs-GO/CPE was applied to determine the G and A content of thermally denatured DNA. As shown in Fig. 5D, the modified electrode gave two well-defined oxidation peaks in the presence of thermally denatured DNA sample at the potentials of 0.84 and 1.12 V due to the oxidation of G and A residues, respectively. The standard addition method was used to determine G and A concentration carefully. In short, 50 μL of thermally denatured DNA solution was added in a 10 mL buffer solution and the peak currents of the G and A were measured. Subsequently, G and A standard solution were added in above mixture and the peak currents of the G and A were recorded again from which the concentrations of G and A in DNA could be evaluated based on the obtained calibration graphs. From these results, the contents of A and G in thermally denatured DNA (in the molar ratio, mol%) and the values of (G + C)/(A + T), were calculated for human blood, hen blood and Anoxybacillus bacteria denatured DNA samples. The results are presented in Table 1. The value of (G + C)/(A + T) for denatured samples obtained over the range from 0.75 to 0.78 which coincided to the standard value of 0.77 (Anu Prathap et al., 2013) and indicating the modified electrode had the same performance as the reported.

3.12.2. Analysis of cancer patient' blood DNA sample

In the present paper, the cancer patient' blood DNA was also investigated. The value of (G + C)/(A + T) for bladder cancer patient' blood DNA sample was obtained 1.21. As mentioned in introduction section, the value of (G + C)/(A + T) in cancer patient' DNA was not in agreement with standard value of 0.77. These observations demonstrate that the ds-DNA/p(L-Cys)/Fe_3O_4 NPs-GO/CPE can not only determine normal DNA bases, but also is able to detect poor changes in the DNA bases and furthermore to evaluate the damaged DNA sample.

4. Conclusions

In this paper, simultaneous electrochemical determination of G and A using ds-DNA/p(L-Cys)/Fe_3O_4 NPs-GO/CPE was investigated. The ds-DNA/p(L-Cys)/Fe_3O_4 NPs-GO/CPE exhibited higher electrocatalytic activity and higher oxidation peak currents toward the oxidation of analytes, which is attributable to superior conductivity and larger

Table 1
Results of A and G determination in various real samples by DPV.

Sample	G		A		Value of (G+C/A+T)
	Molar ratio (%)	RSD (%)	Molar ratio (%)	RSD (%)	
Human blood DNA	21.60	2.03	28.39	2.05	0.76
Hen blood DNA	21.40	2.05	28.06	2.28	0.75
Anoxybacillus DNA bacteria	21.96	1.92	28.03	2.16	0.78
Bladder cancer patient' blood DNA	26.89	1.26	22.42	2.25	1.11

surface area of the DNA biosensor. In comparison with the previously reported methods for electrochemical determination of G and A, the presented method has many advantages, such as simple fabrication, lower detection limit, high anti-interference ability, low cost and high stability. Under the optimized conditions, the proposed DNA biosensor has a strongly electrocatalytic capability for individual and simultaneous determination of analytes. For simultaneous determination, the wide linear range of 0.01–25 μM for G and A were deduced and the limit of detections were calculated to be 1.59 and 3.48 nM, respectively. Life time of the biosensor is 85 measurements with current loss less than 10%. The fabricated electrode showed excellent reproducibility and stability for determination of G and A in human blood, hen blood and Anoxybacillus bacteria denatured DNA samples and evaluation of DNA bases damage. Thus, this biosensor promises to be a good platform for efficient electrochemical analysis.

Acknowledgment

The authors are thankful to the post-graduate office of Guilan University (GU/FC20164) for their support of this work.

Conflict of interest

The authors confirm that this article content has no conflict of interest.

Appendix A. Supplementary material

Supplementary data associated with this article can be found in the online version at http://dx.doi.org/10.1016/j.bios.2017.11.002.

References

Anu Prathap, M.U., Srivastava, R., Satpati, B., 2013. Electrochim. Acta 114, 285–295.
Arvand, M., Gholizadeh, T.M., 2013a. Colloids Surf. B: Biointerfaces 103, 84–93.
Arvand, M., Gholizadeh, T.M., 2013b. Sens. Actuators B Chem. 186, 622–632.
Arvand, M., Hemmati, S., 2017. Sens. Actuators B Chem. 238, 346–356.
Arvand, M., Ghodsi, N., Zanjanchi, M.A., 2015. Biosens. Bioelectron. 77, 837–844.
Chawla, S., Pundir, C.S., 2011. Biosens. Bioelectron. 26, 3438–3443.
Chen, G., Zhao, J., Liu, X., Gao, G., Huang, J., Li, G., 2007. J. Biotechnol. 127, 653–656.
Cho, S., Lee, J.S., Jun, J., Kim, S.G., Jang, J., 2014. Nanoscale 6, 15181–15195.
Ensafi, A.A., Abarghoui, M.M., Rezaei, B., 2014. Sens. Actuators B Chem. 204, 528–535.
Esmaeili, C., Heng, L.Y., Chiang, C.P., Rahman, Z.A., Safitri, E., Marugan, R.S.P.M., 2016. Sens. Actuators B Chem. 242, 616–624.
Feng, L.J., Zhang, X.H., Liu, P., Xiong, H.Y., Wang, S.F., 2011. Anal. Biochem. 419, 71–75.
Ferraz, B.R.L., Leite, F.R.F., Malagutti, A.R., 2016. Talanta 154, 197–207.
Fu, Y., Wang, L., Chen, Q., Zhou, J., 2011. Sens. Actuators B Chem. 155, 140–144.
Gu, T., Wang, J., Xia, H., Wang, S., Yu, X., 2014. Materials 7, 1069–1083.
Huang, K.J., Niu, D.J., Sun, J.Y., Han, C.H., Wu, Z.W., Li, Y.L., Xiong, X.Q., 2011. Colloids Surf. B: Biointerfaces 82, 543–549.
Huang, K.J., Wang, L., Wang, H.B., Gan, T., Wu, Y.Y., Li, J., Liu, Y.M., 2013. Talanta 114, 43–48.
Huang, K.J., Liu, Y.J., Wang, H.B., Wang, Y.Y., 2014. Electrochim. Acta 118, 130–137.
Huang, Y.F., Chang, H.T., 2007. Anal. Chem. 79, 4852–4859.
Kurbanoglu, S., Ozkan, S.A., Merkoçi, A., 2017. Biosens. Bioelectron. 89, 886–898.
Ma, X., Chen, M., 2015. Sens. Actuators B Chem. 215, 445–450.
Ma, X., Wang, Z., Wang, X., Xu, L., 2013. J. Solid State Electrochem. 17, 661–665.
Mashhadizadeh, M.H., Karami, Z., 2011. J. Hazard. Mater. 190, 1023–1029.
Mirmomtaz, E., Ensafi, A.A., Soleimanian-Zad, S., 2009. Electrochim. Acta 54, 1141–1146.
Mohammad-Rezaei, R., Razmi, H., Abdollahi, V., Matin, A.A., 2014. Anal. Methods 6, 8413–8419.
Mokhtari, A., Karimi-Maleh, H., Ensafi, A.A., Beitollahi, H., 2012. Sens. Actuators B Chem. 169, 96–105.
Palecek, E., Bartosik, M., 2012. Chem. Rev. 112, 3427–3481.
Peng, H.P., Hu, Y., Liu, P., Deng, Y.N., Wang, P., Chen, W., Liu, A.L., Chen, Y.Z., Lin, X.H., 2015. Sens. Actuators B Chem. 207, 269–276.
Rezaei, B., Khalili, M., Ensafi, A.A., 2016. Sens. Actuators B Chem. 222, 849–856.
Sundaram, S., Abdul Kadir, M.R., 2017. Electrochim. Acta 224, 475–486.
Tabrizi, M.A., Shamsipur, M., 2015. Biosens. Bioelectron. 69, 100–105.
Wang, J., 2006. Analytical Electrochemistry, 3rd ed. Wiley–VCH, New York.
Wang, Z., Xiao, S., Chen, Y., 2006. J. Electroanal. Chem. 589, 237–242.
Yari, A., Saidikhah, M., 2016. J. Electroanal. Chem. 783, 288–294.
Yu, M., Liang, C., Liu, M., Liu, X., Yuan, Cao, K.H., Che, R., 2014. Mater. Chem. C 2, 7275–7283.
Zeng, L., Zhang, A., Zhu, X., Zhang, C., Liang, Y., Nan, J., 2013. J. Electroanal. Chem. 703, 153–157.
Zhou, Y., Yan, H., Xie, Q., Yao, S., 2015. Talanta 134 (345–259).
Zou, L., Xu, Y., Luo, P., Zhang, S., Ye, B., 2012. Analyst 137, 414–419.